Iranian Journal of Physics Research, Vol. 22, No. 3, 2022
DOI: 10.47176/ijpr.22.3.21378

The role of the cell shapes on the characteristics of a complex earthquake network

E Khodakarami, S Taran, N Asaadi, B Kaki, and H Safari
Department of Physics, Faculty of Science, University of Zanjan, P. O. Box45195-313, Zanjan, Iran

E-mail: nazilaasaadi@znu.ac.ir

(Received 11 December 2021 ; in final form 26 April 2022)

Abstract
We studied the behavior of the earthquake network using the HEALPix spherical pixelization and square cells methods. In the first method, the geographical region is divided into isolatitude rhombic-spherical cells of the same areas using the HEALPix method. In the second method, we divided the geographical region into isolatitude equal areas of the square cells. To construct a network, if an earthquake happens in a cell, that cell will become a node, and two nodes will be connected with an edge for two successive events. The earthquake network is built from Iran's seismic data from 1900 June 12 to 2015 December 12. We determined the Hurst exponent (H = 0.6) due to the rescaled range (R/S) analysis. This value reveals a long temporal correlation in earthquake time-series; therefore, the earthquake system is suggested to be self-organized. We showed that among the five major seismotectonic provinces of Iran (Alborz-Azarbayejan, Kope Dagh, Central-East Iran, Zagros, and Makran), the earthquake network hubs are located in the Zagros region, which is a seismically very active region. According to this result, the Zagros earthquakes affect the surrounding earthquakes. The probability distribution function's power-law behavior with a network built in the pixelization rhombic-spherical cells shows scale free behavior's properties than a network constructed based on the square cells. The mean clustering coefficient's power-law nature with networks built using two methods shows that the earthquake network is scale-free and non-random. We concluded that the rhombic-spherical cell pixelization is a more reliable method for building the large geographical region's earthquake network.

Keywords: complex network, earthquake, HEALpix method, square cell method

1. Introduction

The Iranian territory is one of the most earthquake-prone areas in the world that is frequently affected by devastating earthquakes that cause the loss of life and finances [1, 2, 3, 4]. The high level of seismic activity is a consequence of the convergence of Arabian and Eurasian plates. The continental-continental collision in the west of Iran, along with the Zagros collision and subduction in the south of Iran along the Makran subduction, results from the convergence [5, 6]. The convergence rate measured by GPS varies from 10 mm/yr in Zagros thrust to 28 mm/yr in the Makran subduction zone [7]. Five important seismotectonic provinces of Iran are Alborz-Azarbaijan, Kope Dagh, Central-East Iran, Zagros, and Makran [8]. The highly seismic area Alborz-Azarbayejan in the north and northwest of Iran are part of the northern limit of the orogenic belt Alpine-Himalayan. The appearance of most large-scale earthquakes marks the lowest seismic regions of Kope Dagh in the northeast of Iran. The intraplate environment of Iran is Central-East, and seismic activity is concentrated on seismogenic fault zones. The continental-continental collision zone of Zagros in the southwest of Iran is a very active region with low and moderate-intensity earthquakes. The Makran ocean-continental subduction zone in southeast of Iran presents a significant difference in the seismic behavior between the east and west of Makran [9].

Many natural phenomena (such as earthquakes, solar flares, electric brain signals) behave like a complex system [10, 11]. So far, many methods have been introduced to analyze complex systems, such as time series analysis, chaos theory, nonlinear algebra, and complex networks [12]. Today, complex networks are used as an approach to analyzing real-world phenomena [13, 14], such as earthquakes (see, e.g. [15]) and solar flares (see, e.g. [16, 17]). In recent decades, much research has been done on earthquakes using different

methods. After publishing two entire articles by Abe and Suzuki [18, 19], an important development took place in the study of earthquake complex networks. They divided the areas between Southern California and Japan into small cubes that would be considered as a network vertex if an earthquake occurred in either of these cubes. Two consecutive earthquakes were also defined as a network edge that shows earthquakes' interaction with each other in those cubes. They also found that the earthquake's mainshock can play the role of a hub on the network (hubs definition in [20]). This network construction method extracted some of the characteristics of earthquakes from seismic data and showed that the complex network of earthquakes is small-world and scale-free [18, 19]. They developed their method and extracted valuable information about the mainshock and aftershock as well as the scaling relation of the earthquake network [21, 22, 23]. Other researchers followed this method of constructing a complex network earthquake.

Lotfi and Darooneh studied Iran's earthquakes using the proposed method of constructing a complex earthquake network by Abe-Suzuki to find the effect of cell size on network feature characteristics [24]. They realized the importance of cell size in network characteristics and found that all the topological network features vary as a resolution power. He et al. made minor changes to the Abe-Suzuki method to see the influence of space-time on the earthquake's complex network features [25]. They found that the network has still shown a small-world and scale-free behavior. Chakraborty et al. formed a complex weighted network of earthquakes using the Abe-Suzuki method [26].

In all the above studies and the like, cubic or square divisions have been considered. Given that earthquakes are spatio-temporal phenomena, it is essential to determine each node's exact position to build the network. The cubic division is suitable for flat surfaces, but it makes the area of the cubes different in each latitude when used on spherical surfaces. Moreover, the network structure will be different from the real world.

Gorski et al. proposed a method for dividing spherical surfaces into rhombuses of an equal area at any latitude to analyze the data distributed on spherical surfaces [27]. This method, called Hierarchical Equal Area isoLatitude Pixelization (HEALPix), was developed initially for analyzing cosmological data but can be used for data distributed on any surface. HEALPix uses a set of advanced algorithms to segment spherical surfaces that can divide each spherical surface into cells of the same area in different ways. With the help of this method, several resolutions can be achieved for each spherical surface.

Another well-known and widely used method for studying time series is the visibility graph method, which was introduced by Lacasa et al. [28]. With the help of this computational tool, a time series can be mapped as a graph. This method can be considered a link between the three scientific branches of nonlinear dynamics, graph theory, and time series analysis. As this tool turns any time series into a straightforward mathematical model, regardless of all its complexities, it has been used as a critical solution in many types of research, from financial markets [29] to solar studies [30, 17] and earthquake time-series networks [31].

Telesca and Lovallo applied the visibility graph method in studying Italy's seismicity between 2005 April 16 and 2010 December 31[32]. They showed that the degree distribution has a power-law behavior, and the exponent of the degree distribution obtained between 3 and 3.25. George used the visibility graph method to study Corinth rift seismic catalog data [33]. He showed that minimizing the exponent γ of degree distribution coincides with the time of a significant event (seismic congestion after a large earthquake) in the examined seismic catalog. Khoshnevis et al. used the visibility graph approach to study earthquakes in a small area in northern Iran [34]. In this way, they studied the relationship between earthquake magnitude (m) and b value from the Gutenberg – Richter law. They introduced the visibility graph approach as a suitable alternative for conventional methods for seismic study and earthquake sequences.

In this paper, we constructed the earthquake network using two different cells, rhombic-spherical cells in the first method and the square cells in the second method. We combined the HEALPix, Abe-Suzuki, and visibility graph techniques to make the network more accurate and more realistic in the first method. We used the sequence of events introduced in the Abe-Suzuki method to construct a visibility graph. Then we mapped the location of the visibility graph vertices on the sphere surface using the HEALPix algorithm. This process helped us get a more realistic view of the seismic network mapping on the Earth's surface. In the second method, we used Abe-Suzuki and the visibility graph method to construct the network. The parameters of the earthquake network of Iran were extracted and studied using two methods. We compared the characteristics of the network built based on two approaches.

In Section 2, we present the Earthquake data. Do earthquakes form a complex system? is described in Section 3. Healpix pixelization algorithm is presented in Section 4. In Section 5, we expressed the characteristics of a complex network. Earthquake complex network of Iran is presented in Section 6, and our results and conclusions are presented in Section 7 and Section 8, respectively.

2. Earthquake data set

The seismological data were obtained from the Iranian Seismological Center (IRSC), located at the University of Tehran's Institute of Geophysics (http://irsc.ut.ac. ir/). IRSC consists of 130 stations throughout Iran, with 80 stations equipped with broadband seismographs and 49 stations with short period seismographs and Mashhad's SRO station works with in-well equipment. Only earthquakes of magnitude (m) between 2.9 and 8 (Richter scale) are considered. Occurrence times and geographic coordinates for the data are used to build the earthquake complex network. The data set used includes seisms between 1900 June 12 and 2015 December 12 in

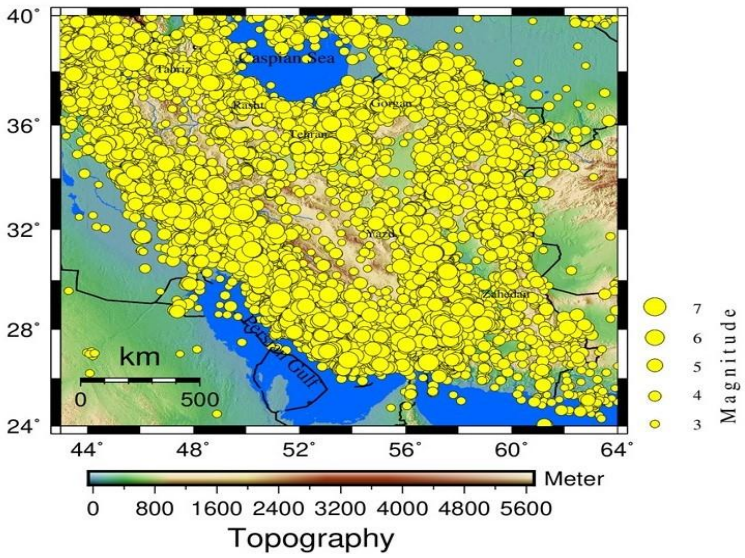

Figure 1. The epicenter of main shocks occurred in Iran from 1900 to 2015. The topography color bar shows the elevation of the selected area. The size of the yellow circles depends on the magnitude of the earthquakes.

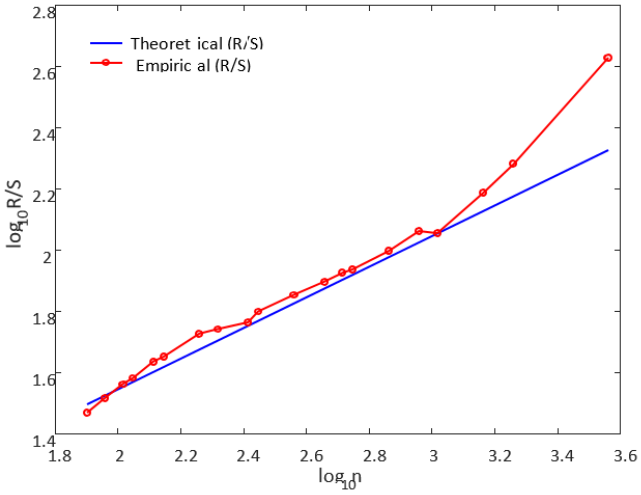

Figure 2. The Hurst exponent (H = 0.6) in applying R/S analysis on time-series of earthquake data.

the region from 40°E to 64°E and 24°N to 44°N. The map of Iran with 20810 earthquakes is shown in figure 1.

3. Do earthquakes form a complex system?

Long-term memory analysis is a robust technique to present the correlation of different times data in an event. Hurst exponent as a result of rescaled range analysis (R/S) and detrended fluctuation analysis (DFA) is a significant parameter of time series characteristics in long-term analysis [35, 36, 37, 30, 17].

R/S method as a statistical technique divides the time-series data with length L into *n* sub-time series ($x_{m,k}$) with length *d*, so that L = nd, and for each sub-time *m* = 1, ...,*d* and *k* = 1,...,*n*, standard deviation is calculated as follow:

$$S_k = \sqrt{\frac{1}{1-d}\sum_{m=1}^{d}(x_{m,k} - \bar{x}_k)}, \qquad (1)$$

in which $\bar{x}_k$ is the mean of sub-series $x_{m,k}$. Each range is rescaled by dividing the range of sub-series (R_k) by the standard deviation of the same portion (R_k/S_k). The average of the rescaled range for all sub-series is

$$(\frac{R}{S})_d = \frac{1}{n}\sum_{k=1}^{n}\frac{R_k}{S_k}, \qquad (2)$$

Weron showd the $(R/S)_d$ has an asymptotically behavior in terms of *n*,

$$(\frac{R}{S})_d \propto n^H, \qquad (3)$$

where H is the Hurst exponent given by a linear fitting in a log-log scale of $(R/S)_d$ versus *n* [35]. Its different ranges give essential information about time-series. Depending on the temporal correlation, H varies between 0 and 1. If 0 < H < 0.5 and 0.5 < H < 1, there is a long-temporal negative and positive correlation, respectively [38, 39, 40, 41].

In the earthquake time-series study, we applied a threshold and omitted less than 2.9 Richter data. We calculate H = 0.6 using R/S analysis on time-series of earthquake data (figure 2). This value shows a long

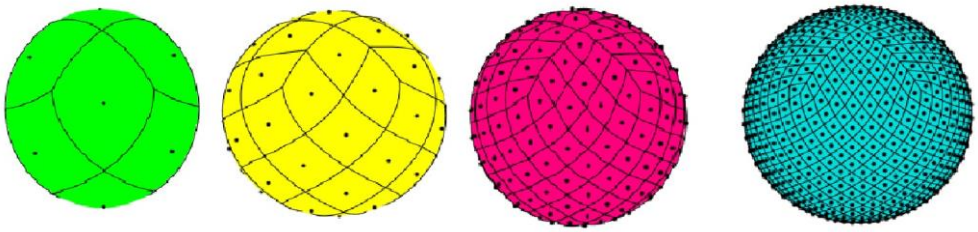

Figure 3. A class of spherical rhombic structures on a sphere. Resolution parameter is 1, 2, 4 and 8 from left to right, respectively.

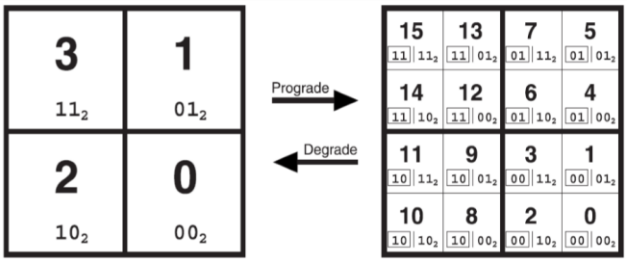

Figure 4. The hierarchical division is shown along with the numbering index of the pixels (squares) (Courtesy by Gorski et al. [27]).

temporal correlation in earthquake time-series and suggests the system is critically self-organized. So this result indicates that the earthquake system has the characteristics of a complex system.

4. HEALPix pixelisation algorithm

HEALPix (the Hierarchical Equal Area isoLatitude Pixelization) is a high-precision framework for the rapid discretization and analysis of distributed data on a sphere. HEALPix includes computational algorithms and visual software to analyze the vast amount of astronomical data distributed on the celestial sphere. Gorski et al. developed this framework to analyze cosmic background radiation data, but it is useable for any data with a spherical structure [27]. Requirements for a spherical pixelization scheme include 1- The hierarchical structure of the database 2- Equal areas for separate partition elements and 3- distribution of these pixels on equal extensions for partitions of the same square on the sphere.

All of these requirements are satisfied by a class with rhombic-spherical structures. Figure 3 shows this kind of class with a rhombic-spherical structure. It is assumed that the hierarchical pixelization divides a sphere surface into four curved squares in base resolution. Each square is divided into four other squares for higher resolutions, and a nested structure is created. The binary indexing is used to square numbering, which in higher resolutions, each square (pixels) inherits its parent pixel index and two new bits to form a new pixel index. Figure 4 shows this type of segmentation along with the pixel index.

Gorski et al. formed an entire class of rhombic-spherical structures on the sphere, using two parameters N_θ and N_φ in a constrained $\cos(\theta_*) = \frac{N_\theta - 1}{N_\varphi}$ where N_θ is the number of base pixel layers between the north and south poles and N_φ is the number of equatorial base pixel layers [27]. Therefore, the resulting base pixels are divided into polar-north, polar-south, and equatorial pixels. Using the constraint $\theta_* = \cos^{-1}\left(\frac{N_\theta - 1}{N_\varphi}\right)$, in the base division, for N_θ = 3 and N_θ= 4, 12 base pixels including 4 polar-north, polar-south, and 4 equatorial pixels formed on the sphere. θ_* is a constraint in which the polar coordinate angle of the lateral vertices of the equatorial and polar pixels intersect. Iran is located in the first polar-north base pixel. For higher resolution, the hierarchical division is performed within these base pixels. Figure 5 shows the base pixelization with the 2D image.

Obviously, the total number of pixels in base resolution satisfies $N_{base-pix} = N_\theta N_\varphi$, and for higher resolutions $N_{pix} = 12N_{side}^2$, which N_{side} is the resolution parameter ($N_{side} = 2^n = 1, 2, 4, 8, \ldots$). The area of each grid resolution parameter N_{side} is $\Omega_{pix} = 4\pi/12N_{side}^2$. The centers of pixels are isolatitude and each latitude named with a ring. The ring number in terms of the resolution parameters is $N_{ring} = 4N_{side} - 1$. Figure 6 shows these pixels and the rings that the pixel centers located on for different resolution parameters.

5. Characteristics of a complex network

In a complex network, we turn the problem into an analyzable structure for studying a phenomenon's properties by defining a mathematical figure called a graph. Thus, each event's location is a node, and the relationship between each event and the other is considered an edge within a graph. The graphs are categorized as directed, undirected, weighted, and unweighted graphs. The edges do not have a direction in undirected graphs. The weighted graph is a graph in which different numbers are related to each edge of the graph. If all numbers are equal to one, the graph is the unweighted graph. By analyzing the adjacency matrix features, a complex network's topological properties, such as local and global scales, were studied [42, 43]. The adjacency matrix is one way to represent graphs. For a graph *G* with *n* nodes and *m* edges, adjacency matrix *A* is a $n \times n$ matrix in which A_{ij} denoting the number of edges jointing node *i* to node *j*. For directed graphs, if

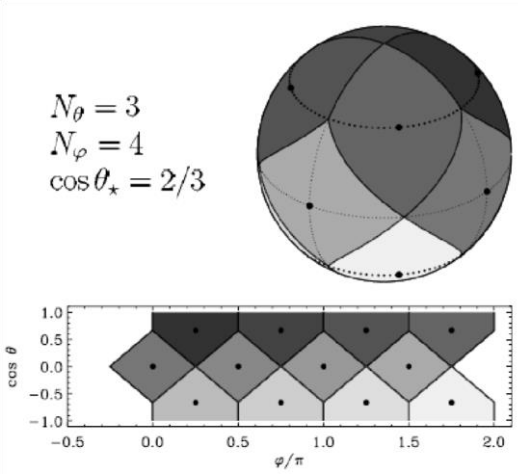

Figure 5. The base pixels are shown with their two-dimensional image (Courtesy by Gorski et al. [27]).

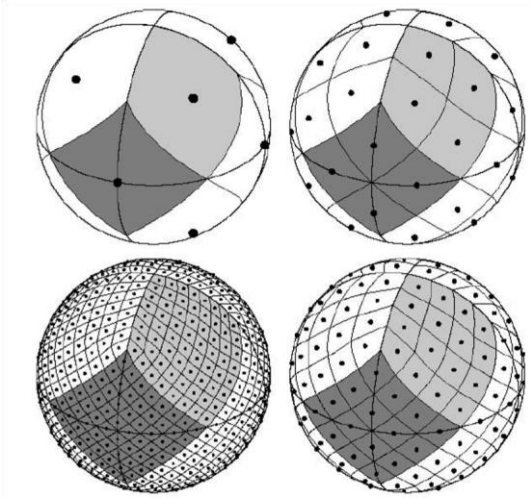

Figure 6. Hierarchical division on the sphere, shown by moving clockwise from top left for resolution 1, 2, 4, and 8, respectively. The sign (·) indicates the centers of each cell on fixed latitudes (Courtesy by Gorski et al. [27]).

there is a connection pointing from node *j* to *i*, $A_{ij} = 1$ and if nodes *i* and *j* aren't connected to each other, $A_{ij} = 0$. The adjacency matrix for undirected graphs is symmetric $A_{ij} = A_{ji}$ and $A_{ii} = 0$. For weighted graphs, the adjacency matrix components A_{ij} are equal to W_{ij}. We used unweighted and undirected adjacency matrices to study the temporal evolution of the earthquake network's parameters. These parameters are the average of local clustering coefficients and probability distribution function (PDF) for the degree of nodes. By using adjacency matrix, we can compute the local clustering coefficients c_i, mean clustering coefficients as follows:

$$c_i = \frac{1}{k_i(k_i-1)} \sum_{l,m=1}^{N} A_{il}A_{lm}A_{mi} \quad , \tag{4}$$

$$c = \frac{1}{N} \sum_{i=1}^{N} c_i, \tag{5}$$

The PDF for degree of nodes is given by:

$$P_k = \frac{n_k}{N} \tag{6}$$

where *N*, k_i,and n_k are node number, degree of node i, adjacency matrix components, and the number of nodes with degree k, respectively.

6. Earthquakes complex network of Iran

According to the complex spatio-temporal relationships between earthquakes, complex network science analyzes the complex system's different features. We used two different methods to construct the earthquake network. In the first method, we used rhombic spherical cells to build the network using the HAELPix method. In the HEALPix method, the Earth's surface is divided into 12 rhombic-spherical cells in the base resolution, in which Iran is located in one of the polar-north cells of this pixelization. In the second method, we consider Iran's total area as the base square cell, and then other divisions are done on this base cell Figure 7.

As the resolution increases, the number of cells increases in both methods. However, according to the base cells in both methods, the number of cells created in square cells is more than rhombic-spherical cells. According to figure 7, for resolution parameter 8, Iran's share is 24 cells in square and 16 cells in HEALPix pixelizations, respectively.

The HEALPix pixelization divides the Earth's sphere into N_{pix} pixels with area A_{pix} for each grid resolution parameter N_{side}, as follow:

$$N_{pix(H)} = 12N_{side(H)}^2, \tag{7}$$

$$A_{pix}(H) = \frac{A_{Earth}}{N_{pix}(H)}, \tag{8}$$

which A_{Earth} is the total area of Earth's surface [27]. Figure 6 shows the HEALPix pixelization results for four parameters. Hereafter, the "H" indicates the HEALPix method.

In square pixelization, the relation between the number of pixels and grid resolution is as follow:

$$N_{pix(s)} = 4^{N_{side(s)}}, \tag{9}$$

in which $N_{side(s)} = 0,1,2,...$, and the pixel's area is given by:

$$A_{pix}(H) = \frac{A_{bs}}{N_{pix(s)}}, \tag{10}$$

that A_{bs} is the base square area for $N_{pix(s)} = 0$. The "s" indicates square method.

The earthquake complex network is considered as an unweighted and an undirected graph. Using the adjacency matrix and according to Abe and Suzuki each pixel is considered as a node, and an edge connects two cells with successive earthquakes [18]. We ignore loops as two successive earthquakes connect in the same cell, and multiple edges between the cells are replaced by one edge for more simplicity.

7. Results

The Iranian plateau is part of the Alps and Himalayas'

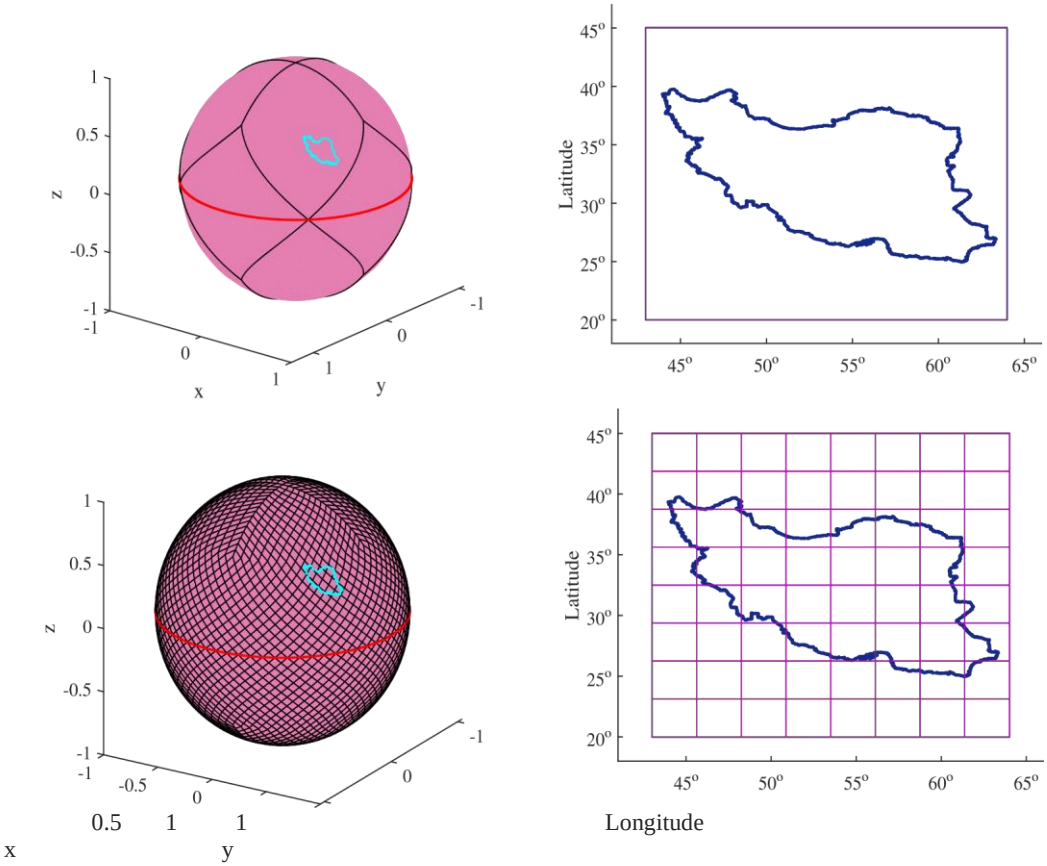

Figure 7. The view of the map of Iran on HEALPix (left) and square (right) pixelization. The top and bottom panels are for the base and eight resolutions, respectively. The HEALPix scheme is on a sphere with a unit radius, and the red rings on HEALPix spheres represent the Earth's equatorial position.

Table 1. The number of nodes and edges are tabulated for six resolution in HEALPix and square methods.

Resolution	HEALPix (node/edge)	Square (node/edge)
128	786/43594	3552/119082
256	2236/92684	7471/157326
512	5175/135490	12611/181241
1024	9697/166480	16690/199292
2048	14604/190320	18998/210010
4096	17922/205461	19969/216216

Orogenic Belt, which presents high seismic activity and a unique deformation scheme. The movement's pressure converging between the Arabian plate and the Turan shield built mountain ranges in Iran [6]. The significant tectonic activity, along with the Zagros collision and the Makran subduction, results from this convergence [44, 45, 46]. As we discussed earlier, one way to improve our understanding of earthquake dynamics is by spatial and temporal analysis of earthquake data. The point of view that we have employed to study the seismic phenomenon is analyzing a complex network created from seismic data.

In all previous articles, the square cell was used many times to divide Iran's geographical region; however, we used the rhombic-spherical cell for the first time to divide the geographical region of Iran. In this work, we have constructed the earthquake network using two methods. The isolatitude rhombic-spherical cells of the same areas are used to partition Iran's geographical area in the first method. In the second method, the isolatitude square cells with the same areas are used to segment the region. In both methods, the cell became a node if there was an earthquake within, and for two successive earthquakes, two nodes connected. We built Iran's earthquake complex network using the occurrence times and geographic coordinates of 20810 events with a magnitude of $2.9 < m < 8$ in the Richter scale. Table 1 presents the earthquake network characteristics built using two methods. As the resolution increases, the number of nodes and edges in each grid increase, but the increasing rate in the square method is faster than HEALPix. We used the unweighted and undirected adjacency matrices to calculate the characteristics of the earthquake network. Calculating the Hurst exponent

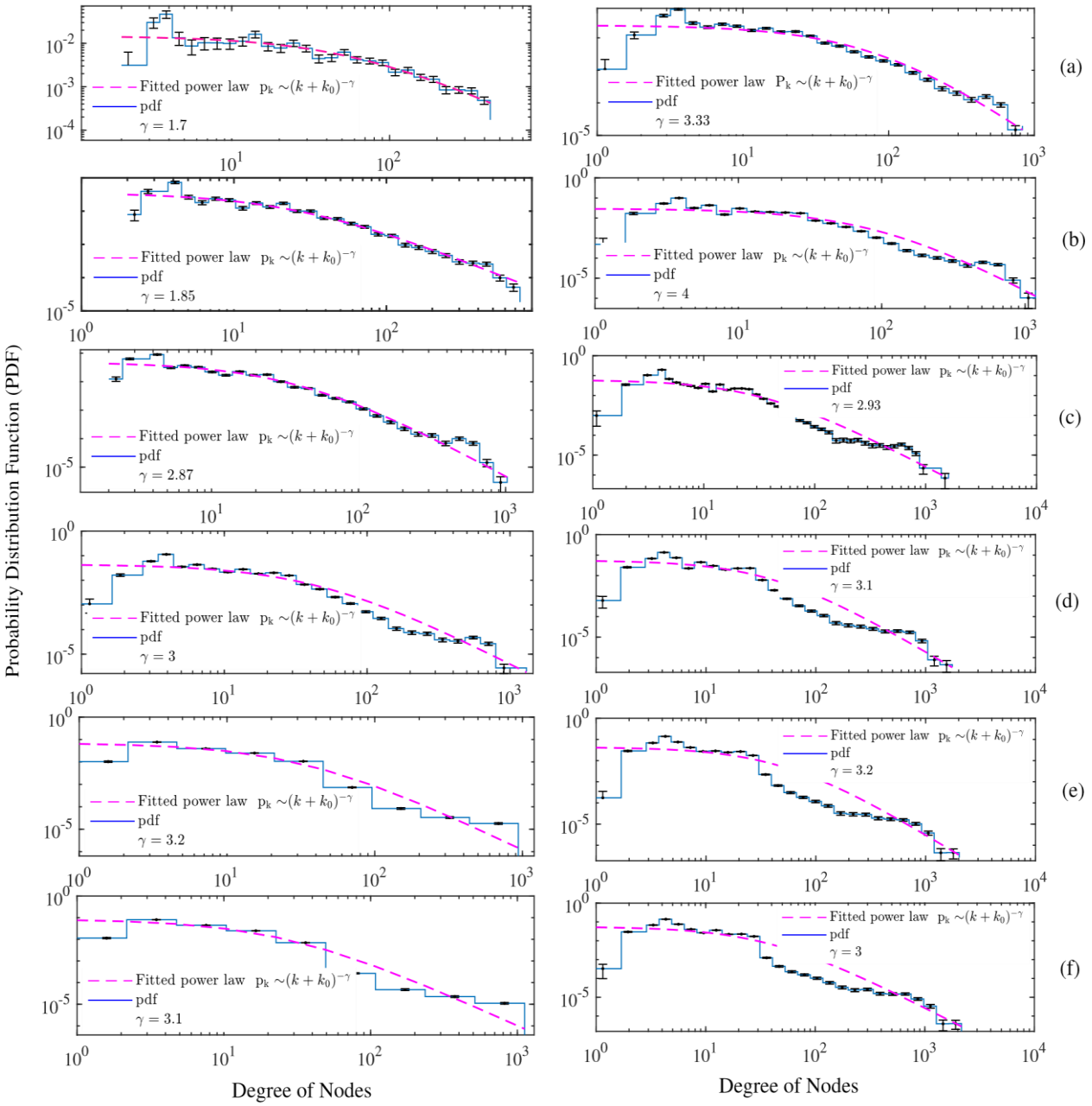

Figure 8. PDFs for the degree of nodes for the HEALPix method (left panel) and square method (right panel) for different resolutions, a) 128, b) 256, c) 512, d) 1024, e) 2048, and f) 4096.

suggest that earthquakes form a self-organized criticality system.

7. 1. Scale-free property of earthquakes network

The power-law nature of the probability distribution function (PDF) of the nodes' degree was found in studies for the world's specific region using square cells for constructing the earthquake network. Abe and Suzuki, Pastén et al. showed the scale-free nature of the PDF in Japan, California, and Chile [18, 19], [21], [47]. We present the PDF of the nodes' degree for two networks built using rhombic-spherical and square cells with the resolution varying from 128 to 4096 (figure 8).

Due to incomplete sampling for finite time-series, the real complex networks do not follow an ideal power-law distribution function for all network sizes; therefore, we use a thresholded power-law distribution [48, 49, 50] in the fitting process as follows:

$$P_k = (k + k_0)^{-\gamma}, \tag{11}$$

where k_0 and γ are thresholded value and the power-law exponent, respectively. The power law exponent values vary from 1.7 to 3.2 and 2.9 to 4.0 for the earthquake networks built using rhombic-spherical and square cells, respectively. By comparing the results for two networks, we see that in the network built using rhombic-spherical cells, the thresholded power-law distribution is well fitted to the nodes' degree of the PDF. Still, in the network constructed with square cells, the thresholded power-law is well fitted for two resolutions, namely 128 and 256. As the resolution increases, the number of divisions increases, and the geographical region's curvature is not seen. So, PDFs are the same for the two networks. In smaller resolution parameters such as 128

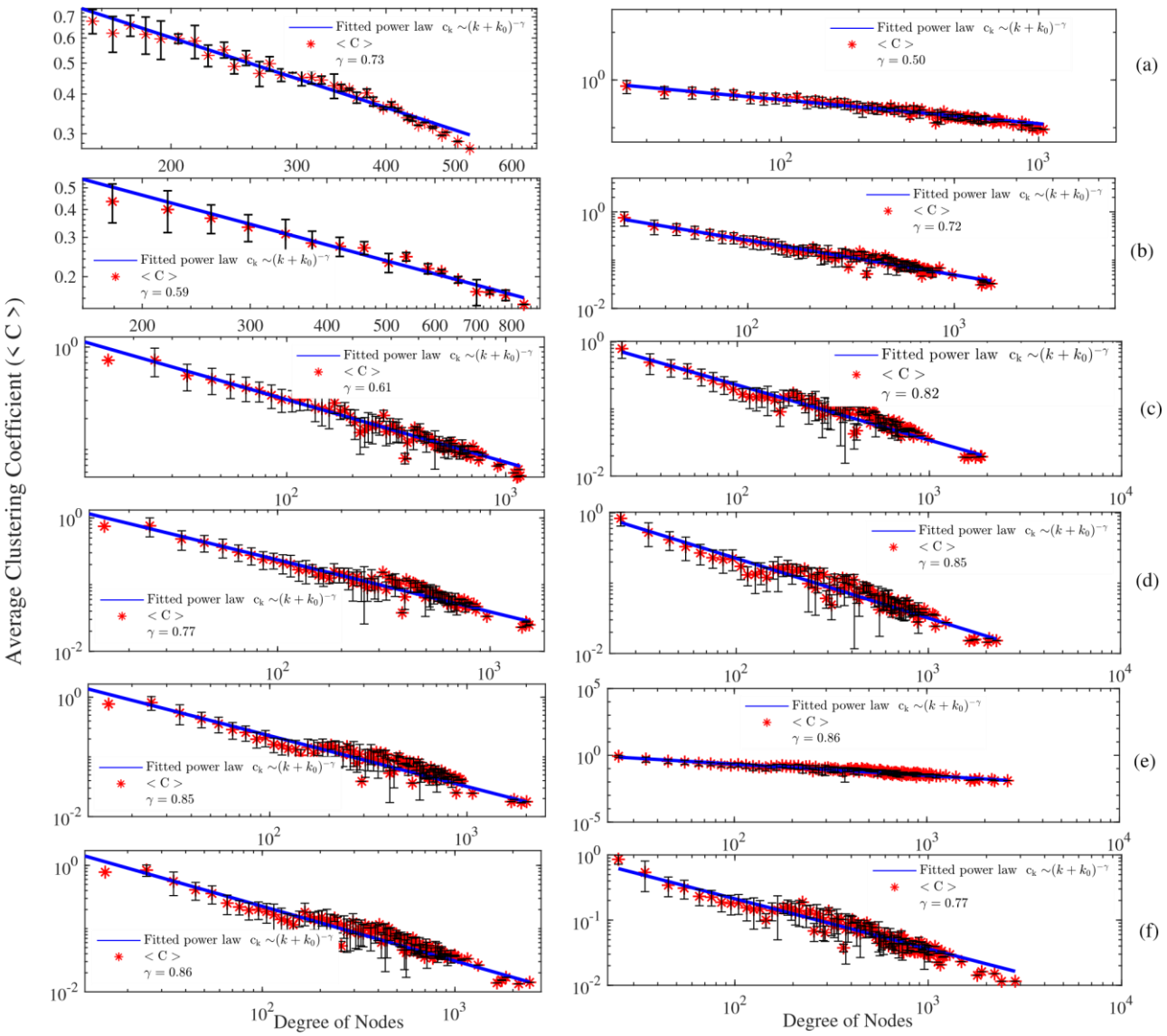

Figure 9. The average local clustering coefficient (<C>) in terms of the degree of nodes for HEALPix method (left panel) and square method (right panel) for different resolutions, a) 128, b) 256, c) 512, d) 1024, e) 2048, and f) 4096.

and 256, there is more difference between the power-law exponent values for two networks. We can conclude that both networks show scale-free behavior, but the network built using the rhombic spherical cells has better results for all resolution parameters. According to Barabási et al. at random networks, the clustering coefficient depends on the average degree of nodes [20]. However, in the real networks, the average local clustering coefficient and degree of nodes have the power-law relationship as $C_k \sim k^{-\gamma}$. Figure 9, presents the average local clustering coefficient in terms of the degree of nodes for two methods of pixelization. Due to the same number of clustering coefficients for the different nodes, the horizontal and vertical lines are revealed in the figure. In this way, analyzing the clustering coefficient in terms of the degree of nodes may be impossible. For this purpose, using mean values of clustering and degrees of nodes in the logarithmic binning intervals are computed (Figure 9). We also used the difference between the maximum and minimum value of the clustering coefficient and the mean value in that box to calculate the error bars. In several studies, the mean clustering coefficient's power-law nature indicate the scale-free and non-random behavior of the earthquake network [19, 51, 52, 53]. We constructed an equivalent random network with the same grid size and edges corresponding to the earthquake network. Figure 10 shows the clustering coefficients of the earthquake network and an equivalent random network in terms of the network size for resolution 128 for two networks built using rhombic and square cells. We used equations (4) and (6) for the clustering coefficient of the earthquakes and random network, respectively. This result shows that the earthquake network is a non-random network.

7. 2. Hubs in the earthquake network of Iran

We obtained a geospatial image of two networks constructed with two pixelization methods as shown in figure 11 (created with Gephi, https://gephi.org). We see that in the geospatial picture of the earthquake network constructed with rhombic spherical cells, the high connectivity nodes (hubs) are located in the Zagros

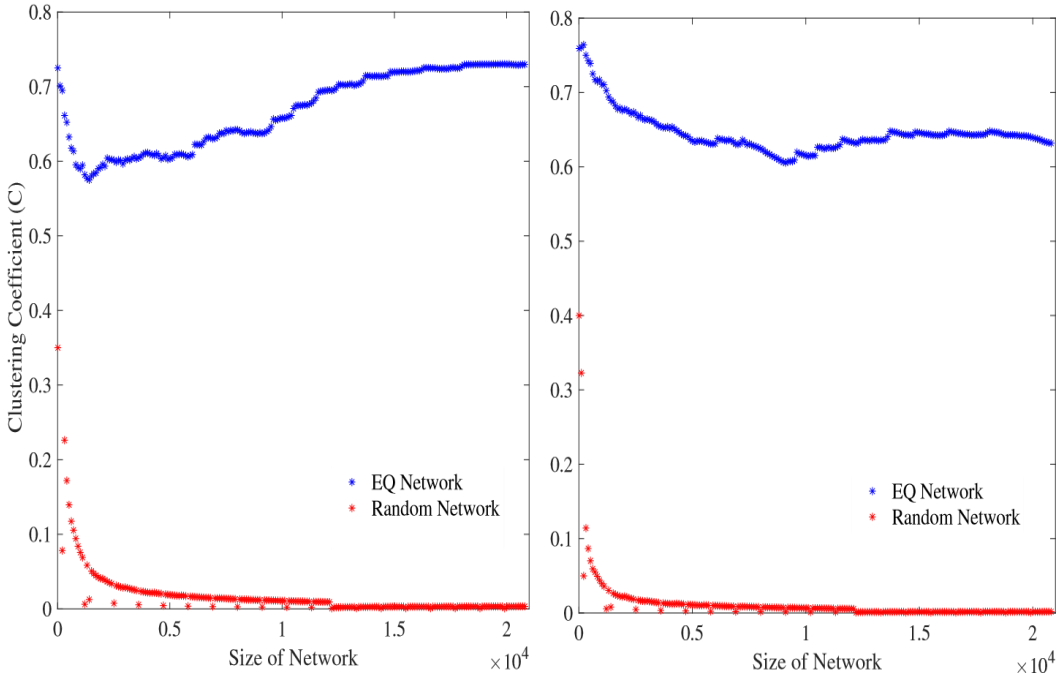

Figure 10. Comparing the clustering coefficient of the earthquakes complex network with equivalent random network for HEALPix(left), square (right) and for resolution parameter 128 is presented.

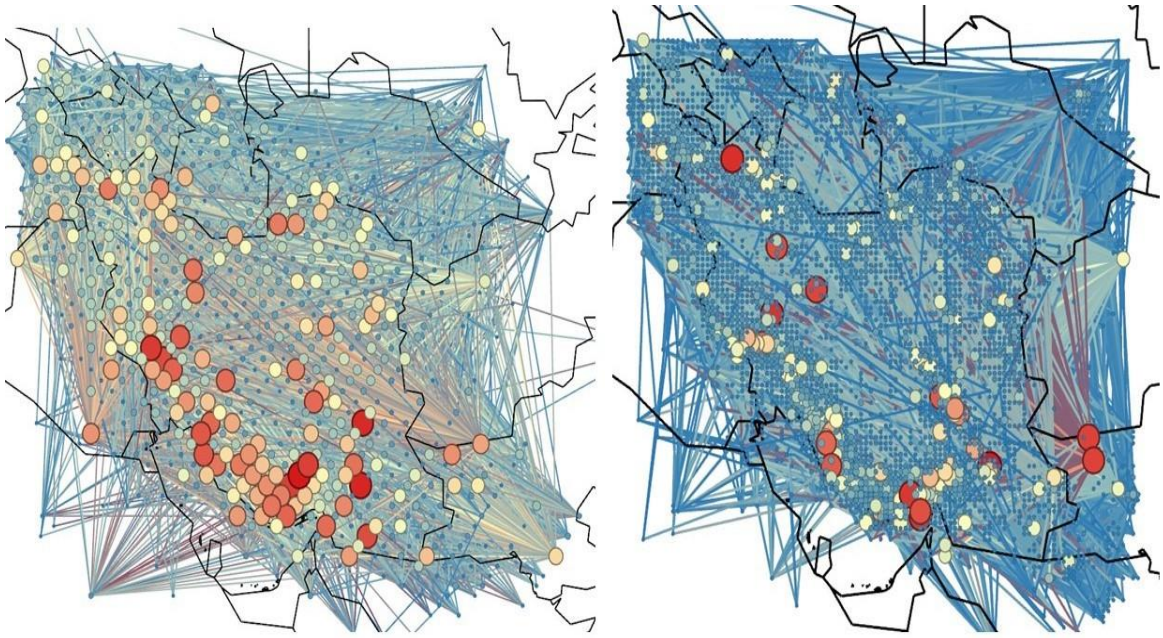

Figure 11. Iran epicenter network's geospatial image: the earthquake network constructed using rhombic spherical cells (right) and square cells (left) with resolution parameter 128. Seismic data taken from 1900 to 2015 and $2.9 < m < 8$. Larger and reddish nodes have a higher number of connections. Most of the hubs are located in the Zagros region.

region. Therefore, earthquakes in the Zagros region affect surrounding earthquakes. This region is a very active seismic zone and the most earthquake-prone area in Iran [9]. However, the same results were not observed in the network built using square cells. In the network built using square cells with increasing the resolution, the number of nodes increases rapidly than the network built using rhombic spherical cells.

The geographical region will segment with smaller cells with increasing the nodes, so this network has additional and unnecessary nodes and edges. In this case, nodes lose their hub nature.

8. Conclusions

We built the Iran earthquake network using two pixelization methods and compared the network's parameters' behavior. To construct the earthquake network, we used the occurrence times and geographic coordinates of 20810 events between 1900 June 12 and 2015 December 12. The undirected and unweighted adjacency matrix is used to determine the PDF of the nodes' degree and clustering coefficient of the network. The Hurst exponent value (H = 0.6) for the Iran earthquake time series suggests that the earthquake

system is a self-organized criticality with a long temporal correlation.

The power-law behavior of the PDF of the nodes' degree for two networks shows the network is scale-free. However, in the network constructed with rhombic-spherical cells, the thresholded power-law is fitted to the PDF better than the network built using square cells. The power-law nature of the average local clustering coefficient presents the network is non-random and scale-free. We found earthquake network hubs are located in the Zagros region in the network built with rhombic-spherical cells. Zagros is among the youngest and most active continental collision zones in southwest Iran [54]. Comparing the results for both constructed networks, we concluded that the network made with the rhombic-spherical cells has better outcomes for network characteristics. The first reason is related to the number of nodes and edges of the networks. By increasing the resolution, the number of nodes increases, so several earthquakes on one cell are divided between several cells and the number of connections increases. As a result, when the geographical region is divided into tiny cells, the nodes will lose their ability to become hubs. The second reason is the power-law behavior of the PDF of the nodes' degree.

There is better fitting between the thresholded power-law and the PDF in the network made with rhombic-spherical cells for all resolutions. But in the network built using square cells just for two resolutions, there is good fitting. The third reason is the position of hubs. In the network built using rhombic-spherical cells, hubs are located in the Zagros region, an essential region in seismic studies. This paper's important outcome is that the rhombic-spherical cell pixelization is a more reliable method for building the large geographical area's earthquake network.

Acknowledgements

The authors would like to thank the Iranian Seismological Center, Institute of Geophysics, University of Tehran for the earthquake data of Iran.

Data statement

The data that support the findings of this study are openly available in the Iranian Seismological Center (IRSC) at the University of Tehran/Iran (http://irsc.ut.ac.ir/index.php?lang=en).

References

1. M Berberian and S Arshadi, *The Geological Survey and Mineral Exploration of Iran* **39** (1976) 397.
2. M Berberian, "*Zagros Hindu Kush Himalaya Geodynamic Evolution"* Geodynamics Series (1981).
3. F Kamranzad, H Memarian, and M Zare, *ISPRS International Journal of Geo-Information* **9** (2020) 430.
4. F Berberian, *et al*., *Journal of the Geological Society* **139** (1982) 605.
5. M A Khanban, *et al*., *Journal of Geodynamics* **143** (2021) 101812.
6. T Shirzad, M A Riahi, and M S Assumpção, *Scientific Reports* **9** (2019) 1.
7. N Mirzaei, G Mengtan, and C Yuntai, *Journal of Earthquake Prediction Research* **7** (1998) 465.
8. N Tahernia, *et al*., *Journal of Earth System Science* **121** (2012) 463.
9. P Bak, "*How nature works: the science of self-organaized criticality"* Springer Science & Business Media (1996).
10. R Shcherbakov, D Turcotte, and J Rundle, "*Treatise on Geophysics Volume 4: Earthquake Seismology"* Elsevier (2015)
11. R Shcherbakov, D Turcotte, and J Rundle, *Bulletin of the Seismological Society of America* **96** (4B), S376
12. G W Flake, "*The Computational Beauty of Nature, Computer Explorations of Fractals, Chaos, Complex Systems, and Adaptation"* MIT Press (2000).
13. S Dorogovtsev and J Mendes, *Advances in Physics* **51** (2002) 1079.
14. L D F Costa, *et al*., *Advances in Physics* **60** (2011) 329.
15. N Lotfi, A H Darooneh, and F A Rodrigues, *Chaos: An Interdisciplinary Journal of Nonlinear Science* **28** (2018) 063113.
16. A L Barabasi, *Linked: The New Science of Networks* (2003) 409.
17. A Gheibi, H Safari, and M Javaherian, *The Astrophysical Journal* **847** (2017) 115.
18. S Abe and N Suzuki, *Europhysics Letters* **65** (2004) 581.
19. S Abe and N Suzuki, *Physica* A*: Statistical Mechanics and its Applications* **337** (2004) 357.
20. A L Barabási, "*Network Science"* Cambridge University Press Cambridge (2016).
21. S Abe and N Suzuki, *Physical Review* E **74** (2006) 026113.
22. S Abe and N Suzuki, *Physica* A **388** (2009) 2511.
23. S Abe and N Suzuki, *Brazilian Journal of Physics* **39** (2009) 428.
24. N Lotfi and A Darooneh, *The European Physical Journal* B **85** (2012) 1.
25. X He, *et al*., *Physica* A **407** (2014) 175.
26. A Chakraborty, G Mukherjee, and S Manna, *Physica* A **433** (2015) 336.
27. K M Gorski, *et al*., *The Astrophysical Journal* **622** (2005) 759.
28. L Lacasa, *et al*., *The Astrophysical Journal* **105** (2008) 4972.
29. E Zhuang, M Small, and G Feng, *Physica* A **410** (2014) 483.
30. F Daei, H Safari, and N Dadashi, *The Astrophysical Journal* **845** (2017) 36.
31. R V Donner and J Donges, *Acta Geophysica* **60** (2012) 589.

32. L Telesca and M Lovallo, *Europhysics Letters* **97** (2012) 50002.
33. H George, *Pure and Applied Geophysics* **97 (**2017**)** 50002.
34. N Khoshnevis, *et al*., *Pure and Applied Geophysics* **174** (2017) 4003.
35. R Weron, *Physica* A*: Statistical Mechanics and its Applications* **312** (2002) 285.
36. B Mandelbrot, *Zeitschrift für Wahrscheinlichkeitstheorie und Verwandte Gebiete* **31** (1975) 271.
37. N Alipour and H Safari, *The Astrophysical Journal* **807** (2015)175.
38. M S Granero, J T Segovia, and J G Pérez, *Physica* A*: Statistical Mechanics and its Applications* **387** (2008) 5543–5551
39. S K Mitra, *Asian Social Science* **8** (2012) 111.
40. M J Aschwanden, *et al*., *Space Science Reviews* **198** (2016) 47.
41. R Ceballos and F Largo, *arXiv:1805.08931* **3, 8** (2018) 424.
42. T H Cormen, *et al*., "*The Knuth-Morris-Pratt Algorithm"* MIT Press (2001)
43. M V Steen, "*Graph Theory and Complex Networks: An Introduction"* Maarten Van Steen (2010).
44. A Şengör, *Geological Society, London, Special Publications* **49** (1990) 797.
45. B Walker, *et al*., *Conservation Ecology* **6** (2002).
46. T Shirzad, *Geophysical Journal International* **217** (2019) 190.
47. D Pastén, *et al*., *arXiv: 100505548* (2012).
48. M Aschwanden, *The Astrophysical Journal* **814** (2015)19.
49. N Farhang, H Safari, and M Wheatland, *The Astrophysical Journal* **859** (2018) 41.
50. N Farhang, M Wheatland, and H Safari, *The Astrophysical Journal Letters* **883** (2019) L20.
51. S Abe and N Suzuki, *The European Physical Journal B Condensed Matter and Complex Systems* **44** (2005)115.
52. S Abe and N Suzuki, *Nonlinear Processes in Geophysics* **13** (2006) 145.
53. S Abe and N Suzuki, *The European Physical Journal* B **59** (2007)93.
54. Z Shomali, *et al*., *Geophysical Journal International* **187** (2011) 394.